Acta Pharmacologica Sinica (2017) 38: 874–884
 1671-4083/17
www.nature.com/aps

Original Article

# Molecular design and synthesis of self-assembling camptothecin drug amphiphiles

Andrew G CHEETHAM[1, 2], Yi-an LIN[1, 2], Ran LIN[1, 2], Honggang CUI[1, 2, 3, 4, *]

*[1]Department of Chemical and Biomolecular Chemistry and [2]Institute for NanoBioTechnology (INBT), Johns Hopkins University, Baltimore, MD 21211, USA; [3]Department of Oncology and Sidney Kimmel Comprehensive Cancer Center, Johns Hopkins University School of Medicine, Baltimore, MD 21205, USA; [4]Center for Nanomedicine, The Wilmer Eye Institute, Johns Hopkins University School of Medicine, Baltimore, MD 21231, USA*

**Abstract**

The conjugation of small molecular hydrophobic anticancer drugs onto a short peptide with overall hydrophilicity to create self-assembling drug amphiphiles offers a new prodrug strategy, producing well-defined, discrete nanostructures with a high and quantitative drug loading. Here we show the detailed synthesis procedure and how the molecular structure can influence the synthesis of the self-assembling prodrugs and the physicochemical properties of their assemblies. A series of camptothecin-based drug amphiphiles were synthesized via combined solid- and solution-phase synthetic techniques, and the physicochemical properties of their self-assembled nanostructures were probed using a number of imaging and spectroscopic techniques. We found that the number of incorporated drug molecules strongly influences the rate at which the drug amphiphiles are formed, exerting a steric hindrance toward any additional drugs to be conjugated and necessitating extended reaction time. The choice of peptide sequence was found to affect the solubility of the conjugates and, by extension, the critical aggregation concentration and contour length of the filamentous nanostructures formed. In the design of self-assembling drug amphiphiles, the number of conjugated drug molecules and the choice of peptide sequence have significant effects on the nanostructures formed. These observations may allow the fine-tuning of the physicochemical properties for specific drug delivery applications, *ie* systemic *vs* local delivery.

**Keywords:** camptothecin; chemotherapy; peptides; self-assembly; drug amphiphiles; prodrugs; nanomedicine

*Acta Pharmacologica Sinica* (2017) 38: 874–884; doi: 10.1038/aps.2016.151; published online 6 Mar 2017

## Introduction

The use of peptides in therapeutic applications, either as drugs themselves[1–3] or as a delivery vector for another bioactive agent[4–12], is a widely explored area within the drug delivery community, especially now that their synthesis has become more facile and cost effective[13, 14]. The versatility in peptide design that the twenty naturally occurring amino acids offer, coupled with the potential for high affinity associations toward target receptors, make their usage highly attractive, especially in the creation of bioactive supramolecular nanomaterials[15–30]. In particular, the attachment of anticancer drugs to small peptides is expected to offer a number of advantages, such as greater aqueous solubility and improved biodistribution through targeting and modified pharmacokinetics. However, while their larger brethren, antibody–drug conjugates, have been introduced into clinical use[31–33], and a number of purely peptide-based drugs are on the market[34], peptide–drug conjugates for cancer therapy are lagging behind with regards to FDA approval and are still undergoing assessment in clinical trials. The reasons for this may be that peptide–drug conjugates can still suffer from the same pharmacokinetic issues that afflict both peptide and small molecule drugs[35–37], that of rapid excretion, hepatic metabolism and non-specific, premature degradation in plasma during circulation and as such no clear benefit has been seen. Polymer-drug conjugates[38–42], in which many drug molecules are covalently attached to a hydrophilic polymer, offer an alternative approach with improved control over the pharmacokinetic profile as the polymer properties (*eg*, radius of gyration) can be adjusted accordingly to increase circulation time and reduce drug excretion. A key issue with this approach, however, concerns polydispersity both in the polymer size and the number of drug molecules successfully conjugated per polymer chain. The inevitable batch-to-batch variability makes it difficult to accurately

*To whom correspondence should be addressed.
E-mail hcui6@jhu.edu
Received 2016-10-01 Accepted 2016-11-14

characterize the individual properties of each polymer-drug conjugate as only averaged properties can be obtained. As a means to address the shortcomings of both approaches, the use of small molecule prodrugs that can assemble into larger aggregate structures is garnering increasing attention[43–53]. These small molecule prodrugs are designed to assemble into larger discrete nanostructures, combining the small molecular nature with the controlled pharmacokinetics potential offered by larger structures such as polymer-drug conjugates or nanoparticle-based drug delivery systems[54–56].

Herein, we outline the design choices involved in the synthesis of peptide-based drug amphiphiles and demonstrate how changes to this design can be used to influence the physicochemical properties and self-assembled morphology. The efficient production of oligo-peptides is best accomplished using solid-phase synthesis techniques, but the conditions required for their post-synthesis isolation (strong acid and scavengers) can be incompatible with many chemotherapeutics and therefore requires that these be introduced using solution-phase chemistry. This dual approach methodology is therefore necessary if we are to develop a generic modular platform that can be altered to incorporate any peptide or anticancer drug of our choosing, allowing the conjugate to be tailored to a particular therapeutic application. Our proof-of-concept design conjugated the hydrophobic drug, camptothecin[57, 58], onto a β-sheet forming peptide via a reduction-sensitive disulfide linker that, under physiological conditions, assembles into filamentous structures (Figure 1). We will use these and other conjugates to illustrate how the design choices influence the resulting nanodrugs. The great advantage of this approach is that their small molecule nature, in comparison to macromolecules, means they can be purified to homogeneity by conventional reversed-phase HPLC methods, allowing the drug content to be precisely controlled through the molecular design.

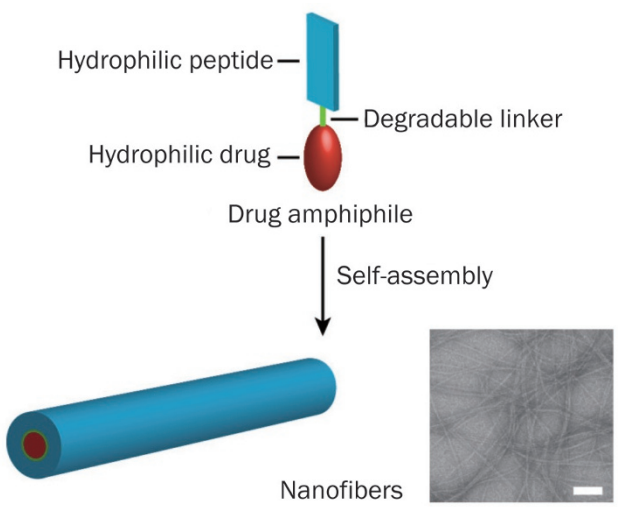


**Figure 1.** Illustration of the drug amphiphile concept. A hydrophilic peptide is conjugated to a hydrophobic drug via a degradable linker. Under physiological conditions, the synthesized drug amphiphiles described self-assemble into nanofibrous structures with a core micelle structure as shown in the representative transmission electron microscopy (TEM) image of mCPT-buSS-Tau (scale bar is 100 nm).

## Materials and methods

### Materials

Fmoc amino acids (unless otherwise stated) and coupling reagents (HBTU or HATU) were purchased from Advanced Automated Peptide Protein Technologies (AAPPTEC, Louisville, KY, USA). Rink Amide MBHA resin and Fmoc-Lys (Fmoc)-OH were obtained from Novabiochem (San Diego, CA, USA). Camptothecin was purchased from AvaChem Scientific (San Antonio, TX, USA) and all other reagents were sourced from Sigma-Aldrich (St Louis, MO, USA) or VWR (Radnor, PA, USA).

### Instruments and methods

RP-HPLC was performed on a Varian ProStar Model 325 HPLC (Agilent Technologies, Santa Clara, CA, USA) equipped with a fraction collector. Preparative separations utilized a Varian PLRP-S column (100 Å, 10 μm, 150 mm×25 mm), whilst analytical HPLC used a Varian Pursuit XRs $C_{18}$ column (5 μm, 150 mm×4.6 mm). Water and acetonitrile containing 0.1% $v/v$ TFA were used as the mobile phase. Purified molecules were lyophilized using a FreeZone -105 °C 4.5 L freeze dryer (Labconco, Kansas City, MO, USA). Mass spectrometric data for characterization was acquired using either a Finnigan LCQ ion trap mass spectrometer (Thermo-Finnigan, Waltham, MA, USA) for ESI-MS or Autoflex III Smartbeam (Bruker, Billerica, MA, USA) for MALDI-Tof MS using α-cyano-4-hydroxycinnamic acid as the matrix. LC-MS analysis was performed using a Thermo-Finnigan Surveyor LC-MS system equipped with a PDA spectroscopic detector and an LCQ Fleet Ion Trap Mass spectrometer. Chromatographic separation was carried out using an Agilent Eclipse Plus C18 column (50 mm×2.1 mm, 1.8 μm), eluting with a water-acetonitrile gradient containing 0.1% $v/v$ formic acid. Data was processed using Thermo XCaliber software. Bruker Avance 300 or 400 MHz FT-NMR spectrometers were used for the acquisition of $^{1}H$ and $^{13}C$ NMR spectra.

### Peptide synthesis

The peptides Ac-CGVQIVYKK-$NH_2$ (mCys-Tau), $(Ac\text{-}C)_2$-KGVQIVYKK-$NH_2$ (dCys-Tau), and $[(Ac\text{-}C)_2K]_2$KGVQIVYKK-$NH_2$ (qCys-Tau) were synthesized using a combination of automated and manual Fmoc-solid phase synthesis techniques (Scheme 1). A Focus XC automated peptide synthesizer (AAPPTEC, Louisville, KY, USA) was used for the synthesis of Fmoc-GVQIVYKK-Rink, using 20% 4-methylpiperidine in DMF for Fmoc deprotections and amino acid/HBTU/DIEA (4:4:6 relative to the resin) in DMF for couplings (with 2 min activation time and 1 h reaction time), further modifications were then carried out manually. For dCys-Tau and qCys-Tau, the branching lysines were introduced using Fmoc-Lys(Fmoc)-OH/HATU/DIEA (4:4:6 relative to each reactive amine), coupling until a negative Kaiser test was obtained, requiring

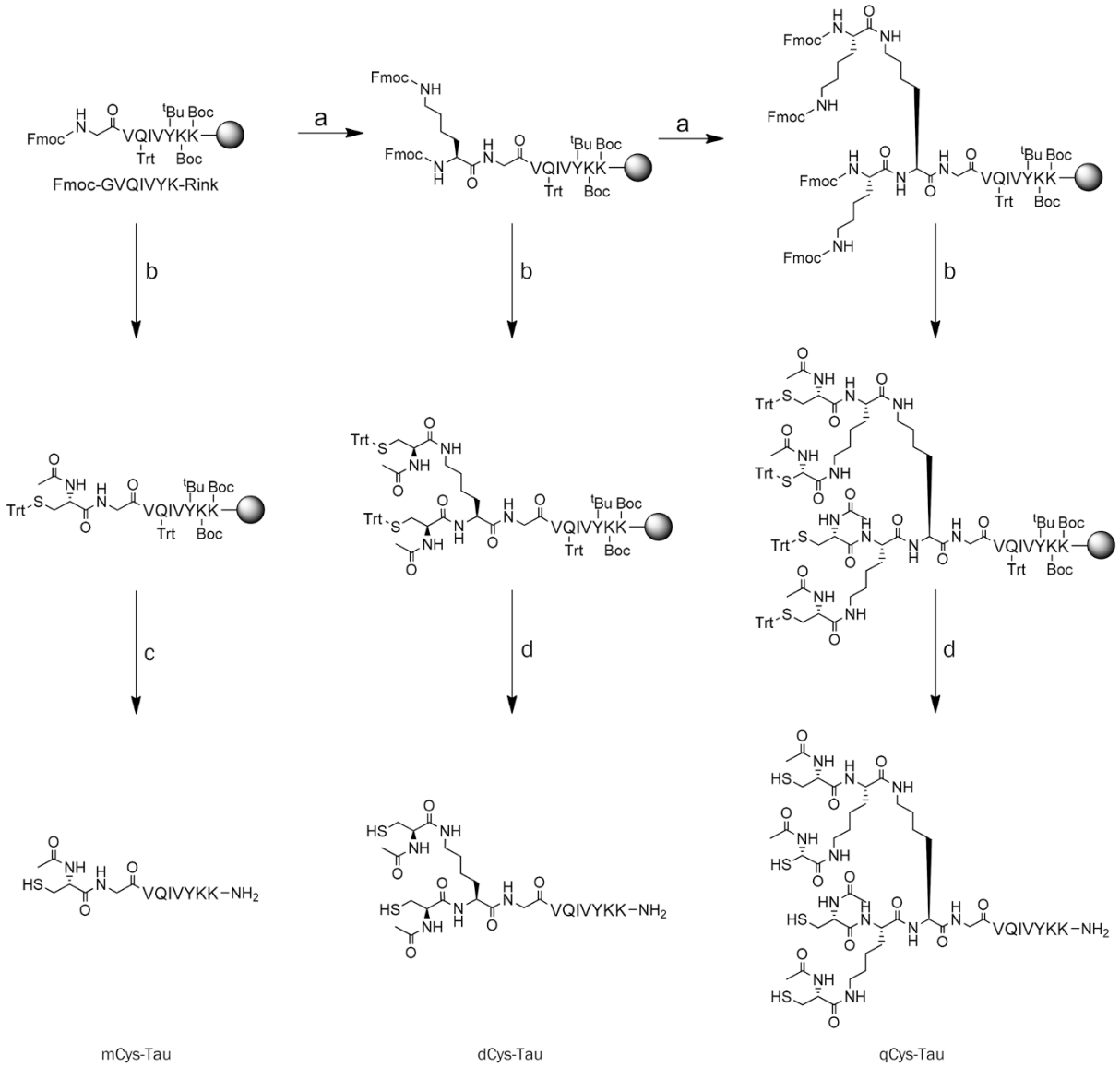


**Scheme 1.** Solid-phase synthesis of the cysteine-functionalized Tau precursor peptides. Fmoc-GVQIVYKK-Rink was created using an automated peptide synthesizer and further modified by manual synthesis techniques. Reaction conditions: (a) (i) 20% 4-methylpiperidine in DMF, (ii) Fmoc-Lys(Fmoc)-OH, HATU, DIEA (4:3.98:6 per amine); (b) (i) 20% 4-methylpiperidine in DMF, (ii) Fmoc-Cys(Trt)-OH, HATU, DIEA (4:3.98:6 per amine), (iii) 20% 4-methylpiperidine in DMF, (iv) 20% acetic anhydride in DMF, DIEA; (c) TFA, TIS, $H_2O$ (95:2.5:2.5); (d) TFA, TIS, $H_2O$, EDT (90:5:2.5:2.5).

extended reaction times and on occasion repeated reaction with fresh reagents. Cysteine incorporation for all three peptides was achieved using Fmoc-Cys(Trt)-OH/HATU/DIEA (4:4:6 relative to each reactive amine). Acetylation was carried out manually using 20% *v*/*v* acetic anhydride in DMF after *N*-terminal Fmoc deprotection.

Peptides were cleaved from the resin using the standard cleavage solution of TFA/TIS/$H_2O$ (95:2.5:2.5) for 2 h, with the exception of dCys-Tau, and qCys-Tau, which used TFA/TIS/$H_2O$/EDT (90:5:2.5:2.5). Cleaved peptides were isolated by trituration into cold diethyl ether, followed by filtration and drying under suction. All peptides were purified to >95% homogeneity by preparative RP-HPLC, with their identity and purity confirmed by MALDI-Tof (Figures S2-S4 in Supplementary Information, SI). The four cysteine-containing peptides were purified by initially dissolving in 1 mL AcOH and then diluting with 0.1% *v*/*v* aqueous TFA to 20 mL.

#### 4-(Pyridin-2-yldisulfanyl)butanoic acid ($HO_2C$-BuSS-Pyr)

This was synthesized using a modification of a previously published method[8]. Briefly, 4-bromobutyric acid (2.0 g, 12.0 mmol) and thiourea (1.06 g, 14.0 mmol) were refluxed in EtOH (50 mL) for 4 h. NaOH (4.85 g, 121 mmol) in EtOH (50 mL) was added and reflux was continued for 16 h. After cooling to room temperature and concentration *in vacuo*, the residue was diluted to 50 mL with water that was extracted twice with

$Et_2O$. The aqueous portion was then acidified to pH 5 with 4 mol/L HCl, giving a cloudy solution that was extracted with $Et_2O$. The organic extracts were dried over anhydrous $Na_2SO_4$ and concentrated to give 4-sulfanylbutyric acid as a clear oil (802 mg, 56%) that was used without further purification. 4-Sulfanylbutyric acid (802 mg, 6.7 mmol) was dissolved in MeOH (5 mL) and added dropwise to a solution of 2-aldrithiol (3.03 g, 13.8 mmol) in MeOH (5 mL), which developed a yellow color. After 3 h, the mixture was purified by RP-HPLC, collecting the major peak and removing the solvents *in vacuo*. The resultant oil was dissolved in $CHCl_3$, dried over $Na_2SO_4$ and solvent removed to give $HO_2C$-BuSS-Pyr as a pale yellow viscous oil (1.02 g, 67%). $^1$H NMR ($CDCl_3$, 400 MHz, 298 K): $\delta_H$ (ppm) 8.59 (d, $^3J_{HH}$=4.6, 1H), 7.91–7.81 (m, 2H), 7.30–7.25 (m, 1H), 2.88 (t, $^3J_{HH}$=7.1, 2H), 2.50 (t, $^3J_{HH}$=7.2, 2H), 2.09-2.00 (m, 2H).

### Camptothecin-4-(pyridin-2-yldisulfanyl)butanoate (CPT-buSS-Pyr)

Camptothecin (200 mg, 574 μmol) was suspended in DCM (32 mL) and dimethylaminopyridine (44 mg, 360 μmol), $HO_2C$-BuSS-Pyr (280 mg, 1.22 mmol) and diisopropylcarbodiimide (436 μL, 2.80 mmol) were added. The mixture was stirred for 36 h, with TLC (3% MeOH in $CHCl_3$) showing complete consumption. The solution was then filtered, diluted with $CHCl_3$ (60 mL), extracted with sat. $NaHCO_3$ (50 mL), brine (50 mL), dried over $Na_2SO_4$ and concentrated *in vacuo*. The residue was purified by flash chromatography using EtOAc (500 mL) then 0.5% MeOH in EtOAc (250 mL). Product fractions were identified by TLC, combined and solvent removed *in vacuo* to give CPT-buSS-Pyr as a pale yellow solid (195 mg, 61%); $^1$H NMR ($CDCl_3$, 400 MHz, 298 K): $\delta_H$ (ppm) 8.43 (d, $^3J_{HH}$=4.2, 1H), 8.40 (s, 1H), 8.23 (d, $^3J_{HH}$=8.6, 1H), 7.94 (d, $^3J_{HH}$=8.2, 1H), 7.84 (m, 1H), 7.70–7.65 (m, 2H), 7.60 (m, 1H), 7.20 (s, 1H), 7.04 (m, 1H), 5.67 (d, $^2J_{HH}$=17.3, 1H), 5.40 (d, $^2J_{HH}$=17.2, 1H), 5.29 (s, 2H), 2.86 (t, $^3J_{HH}$=7.1, 2H), 2.75–2.57 (m, 2H), 2.31–2.03 (m, 4H), 0.97 (t, $^3J_{HH}$=7.5); $^{13}$C NMR ($CDCl_3$, 100 MHz, 298 K): $\delta_C$ (ppm) 172.1, 167.7, 160.3, 157.6, 152.6, 149.9, 149.1, 146.6, 146.1, 137.3, 131.5, 131.4, 130.9, 129.9, 128.63, 128.62, 128.4, 128.3, 120.4, 96.1, 76.2, 67.4, 50.2, 37.7, 32.4, 32.0, 31.2, 24.0, 7.9; MS (MALDI-TOF): 560.065 $[M+H]^+$.

### Synthesis of the drug-amphiphiles

All drug amphiphiles were synthesized by reaction of the peptide cysteine thiol(s) with the activated disulfide of CPT-buSS-Pyr in $N_2$-purged DMSO (Scheme 2), followed by RP-HPLC purification as described below in more detail.

#### *mCPT-buSS-Tau*

mCys-Tau (14.6 mg, 13.5 μmol) was dissolved in an $N_2$-purged DMSO solution CPT-buSS-Pyr (10 mg in 1.50 mL, 17.8 μmol) and shaken overnight. The reaction was diluted to 30 mL with 0.1% *v*/*v* aqueous TFA, giving a slightly viscous solution that was then purified by RP-HPLC. Product fractions were combined and immediately lyophilized. The pale yellow solid obtained was dissolved in 25 mL nanopure water and the product concentration was determined by DTT calibration to be 233 μmol/L (8.9 mg, 43%). The solution was then aliquotted into cryo-vials, lyophilized and stored at -30 °C.

#### *dCPT-buSS-Tau*

dCys-Tau (10.8 mg, 5.0 mmol) was dissolved in an $N_2$-purged DMSO solution of CPT-buSS-Pyr (9 mg in 500 μL, 16.1 μmol) and allowed to react for 3 d. The solution was diluted to 10 mL with 0.1% *v*/*v* aqueous TFA and purified by RP-HPLC. Product fractions were combined and immediately lyophilized. The pale yellow solid obtained was dissolved in 15 mL nanopure water containing 0.1% TFA and 8% acetonitrile and the product concentration was determined by DTT calibration to be 72.9 μmol/L (2.5 mg, 22%). The solution was then aliquotted into cryo-vials, lyophilized and stored at -30 °C.

#### *qCPT-buSS-Tau*

qCys-Tau (3.5 mg, 1.91 μmol) was dissolved in an $N_2$-purged DMSO solution of CPT-buSS-Pyr (10 mg in 500 μL, 17.8 μmol) and allowed to react for 8 d. The solution was diluted to 10 mL with 0.1% *v*/*v* aqueous TFA and purified by RP-HPLC. Product fractions were combined and immediately lyophilized. The pale yellow solid obtained was dissolved in 19.5 mL nanopure water containing 0.05% TFA and 25% acetonitrile and the product concentration was determined by DTT calibration to be 14.2 μmol/L (1.0 mg, 15%). The solution was then aliquotted into cryo-vials, lyophilized and stored at -30 °C.

### Concentration calibration

To determine the CPT concentration of the purified drug amphiphiles, a dithiothreitol (DTT) reduction assay was developed. Briefly, a solution of the conjugate with an approximate concentration in the range 5 to 500 μmol/L was adjusted to pH 7 with a known amount of 0.1 mol/L NaOH. 10 μL of freshly prepared 3 mol/L aqueous DTT was added to 90 μL of the conjugate solution and allowed to stand for 3 h with periodic vortexing. 30 μL of this sample was then mixed with 20 μL of DMSO and analyzed by RP-HPLC (injecting 50 μL so as to completely fill the 20 μL sample loop), measuring the area of the peak due to CPT-buSH. The CPT concentration of the analyzed solution in μmol/L is given by (peak area)/0.2964 (as determined by a calibration curve study of DTT-reduced CPT-buSS-Pyr, section S1.4 in SI). The conjugate concentration of the original solution was calculated based on the applied dilutions and number of CPT molecules the conjugate possesses.

### Transmission electron microscopy (TEM) imaging

A 100 μmol/L aqueous solution of drug amphiphile was prepared from a stock solution of 1 mmol/L conjugate in water. Samples were aged overnight prior to sample preparation. A sample for imaging was prepared by depositing 7 μL of the solution onto a carbon-coated copper grid (Electron Microscopy Services, Hatfield, PA, USA), wicking away the excess solution with a small piece of filter paper. Next, 7 μL of a 2% (wt) aqueous uranyl acetate solution was deposited and the excess solution was carefully removed as above to leave a very

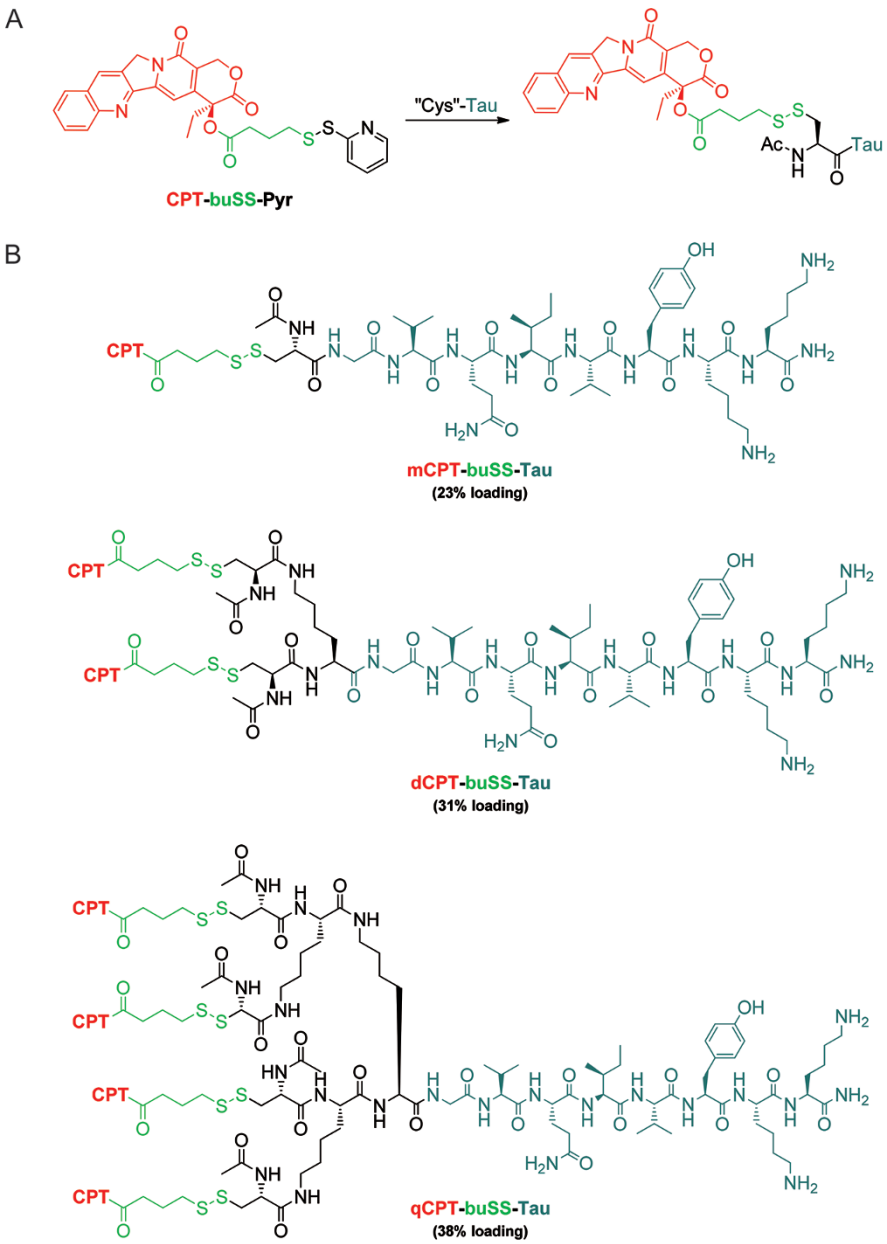


**Scheme 2.** (A) Directed disulfide formation method used to synthesize the described drug amphiphiles and (B) molecular structures of the three drug amphiphiles mCPT-buSS-Tau, dCPT-buSS-Tau and qCPT-buSS-Tau and their respective drug loadings.

thin layer. The sample grid was then allowed to dry at room temperature prior to imaging. Bright-field TEM imaging was performed on a FEI Tecnai 12 TWIN Transmission Electron Microscope operated at an acceleration voltage of 100 kV. All TEM images were recorded by a SIS Megaview III wide-angle CCD camera.

### Cryogenic-TEM (Cryo-TEM) imaging

3–5 μL of the sample solution was placed on a holey carbon film supported on a TEM copper grid (Electron Microscopy Services, Hatfield, PA, USA) that had been pre-treated with plasma air to render the film hydrophilic. A thin film of the sample solution was produced using a Vitrobot with a controlled humidity chamber (FEI). After loading of the sample solution, the lacey carbon grid was blotted using preset parameters and plunged instantly into a liquid ethane reservoir precooled by liquid nitrogen. Vitrified samples were then transferred to a cryo-holder and cryo-transfer stage that was cooled by liquid nitrogen. To prevent sublimation of vitreous water, the cryo-holder temperature was maintained below -170 °C during the imaging process. Imaging was performed on the FEI Tecnai 12 TWIN Transmission Electron Microscope, operating at 80 kV. All images were recorded by a 16 bit 2K×2K FEI Eagle bottom mount camera.

### Circular dichroism (CD)

The CD spectra were recorded on a Jasco J-710 spectropolarimeter (JASCO, Easton, MD, USA) using a 1 mm path length quartz UV-Vis absorption cell (Thermo Fisher Scientific, Pittsburgh, PA, USA). A background spectrum of the solvent was acquired and subtracted from the sample spectrum. Collected data were normalized with respect to sample concentration and β-sheet forming residues.

## Results

### Peptide synthesis

The peptides used in this study were synthesized using standard Fmoc solid-phase peptide synthesis techniques (Scheme 1), employing an automated synthesizer to make the backbone of the sequence –GVQIVYKK-Rink– and manual synthesis techniques to add the requisite cysteine residues. For the mono-Cys peptide, no issues were observed for the coupling of cysteine or during cleavage from the resin when using standard protocols. For both the di- and quad-Cys peptides, however, extended reaction time or double couplings were required for complete reaction to occur. Cleavage also presented a problem and a solution containing a greater amount of the scavenger triisopropylsilane (5% compared to 2.5%), in addition to ethane-1,2-diol (2.5%), was required to obtain the product, otherwise significant degradation to unidentifiable species was found to occur. Purification of these peptides required initial dissolution in acetic acid to avoid the formation of a gelatinous solid that would result upon addition of acidic water to the crude solids.

### Prodrug linker synthesis

The activated disulfide prodrug, CPT-buSS-Pyr, was synthesized by adapting a procedure used to create a similar paclitaxel prodrug[8]. CPT was esterified by reaction with 4-(pyridin-2-yldisulfanyl)butanoic acid in the presence of DIC and DMAP, giving CPT-buSS-Pyr in 61% yield after purification.

### Synthesis of mCPT-buSS-Tau

Reaction of mCys-Tau with an excess of the activated disulfide CPT-buSS-Pyr in $N_2$-purged DMSO was found to give rapid conversion to the desired conjugate, mCPT-buSS-Tau, by both ESI-MS and HPLC analysis (Figures 2A and 3A). After overnight agitation to allow the reaction to go to completion, purification by reversed phase HPLC and subsequent lyophilization of product fractions gave mCPT-buSS-Tau in 43% yield, with >99% homogeneity (by HPLC).

### Synthesis of dCPT-buSS-Tau

The synthesis of the di-conjugate was performed in a similar manner to that of mCPT-buSS-Tau, though a longer reaction time was required to achieve near complete reaction. The formation of the semi-reacted conjugate containing one CPT moiety could be clearly seen (Figures 2B and 3B), with HPLC analysis indicating the formation of the two isomeric forms. Purification as above gave dCPT-buSS-Tau in 22% yield, with >99% homogeneity (by HPLC).

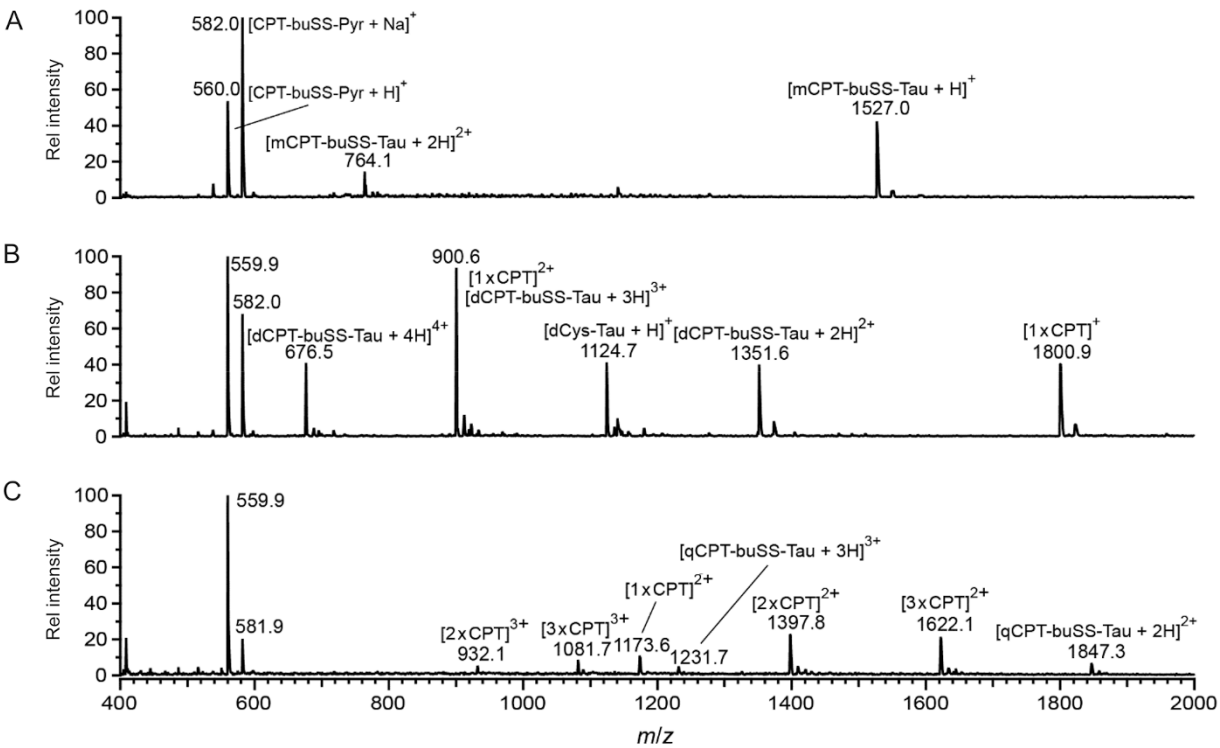


**Figure 2.** ESI-MS analysis of the reaction solutions during drug amphiphile synthesis. mCPT-buSS-Tau after 1 h (A), dCPT-buSS-Tau after 3 h (B), and qCPT-buSS-Tau after 18 h (C). 1×, 2×, and 3× CPT indicate singly, doubly and triply reacted products, respectively.

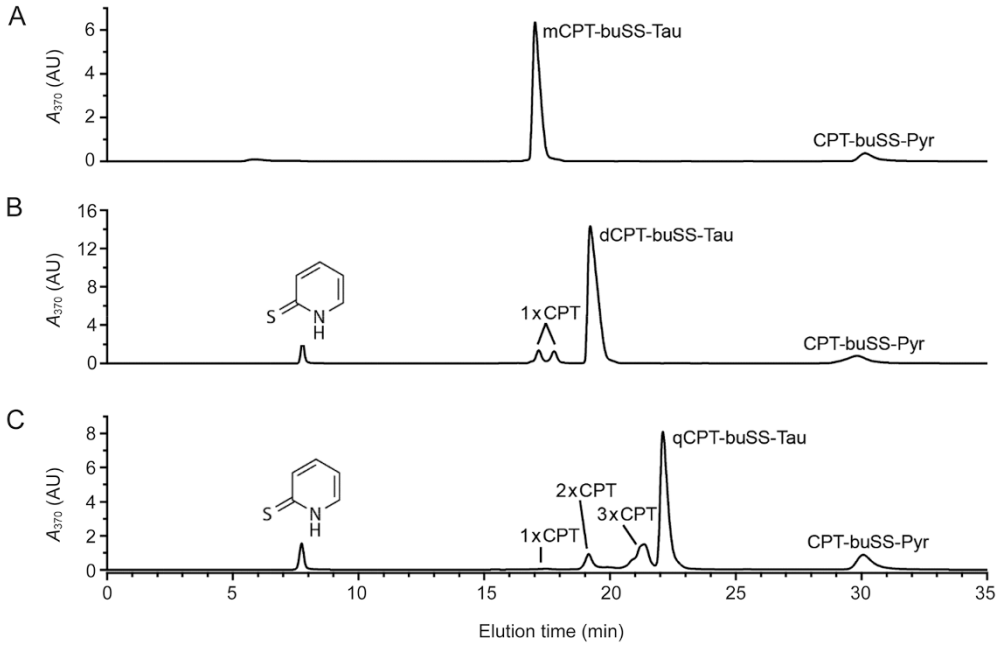


**Figure 3.** Preparative HPLC chromatograms of mCPT-buSS-Tau (A), dCPT-buSS-Tau (B), and qCPT-buSS-Tau (C) showing the reaction products formed during the synthesis of the drug amphiphiles. 1×, 2× and 3× CPT indicate incomplete reaction products.

### Synthesis of qCPT-buSS-Tau

The formation of the quad-conjugate was observed to take much longer to occur, even with a larger excess of CPT-buSS-Pyr, ESI-MS analysis (Figure 2C) clearly showed the formation of mono-, di- tri- and quad-reacted species after overnight agitation. Despite the decreased rate of reaction, the cysteine thiols remained reactive and after 8 d significant conversion had been achieved (Figure 3C). Purification was therefore performed as before, giving qCPT-buSS-Tau in 15% yield, with >99% homogeneity (by HPLC).

## Discussion

### Drug amphiphile design and synthesis

Our approach for the synthesis of peptide-based amphiphilic drug conjugates is the attachment of the hydrophobic chemotherapeutic agent to a peptide with overall hydrophilicity via a biodegradable linker (Figure 1). When designing such a conjugate, there are a number of important points that must be considered. First, the peptide can be chosen so as to influence both the assembly properties of the conjugate and the surface chemistry of the assembled nanostructure[59]. The preferred secondary structure that the peptide adopts can strongly influence the final assembly morphology, with β-sheet-forming peptides preferentially giving one-dimensional (1D) fibrous structures[60, 61], whereas other secondary structures could give rise to micelles or vesicles[62, 63]. Peptide-based epitopes or other moieties could also be incorporated so as to bestow further functionality upon the drug nanostructures, such as targeting[18, 64–66] and stealth capabilities[67, 68].

Second, the linker choice is important as release of the free drug is essential if a cytotoxic effect is to be induced. The development of degradable linker groups has been ongoing for several decades and there are many examples in the literature that can be utilized, including acid-sensitive[69], enzyme-cleavable[70, 71], and reducible[72, 73].

Third, since many chemotherapeutics can be sensitive to strongly acidic conditions, the use of conjugation methods for post-cleavage attachment to the peptide is often required since the coupling cannot be performed on-resin. These conjugation methods necessitate reaction mechanisms that must be selective and efficient so as to minimize side-reactions. A multitude of reactions for the conjugation of synthetic entities to proteins have been developed that satisfy these conditions and can be readily applied for the purpose of peptide–drug conjugation. Examples of these include directed disulfide formation[74], thiolene reaction[75] or copper-assisted azide-alkyne cycloaddition (CuAAC)[76]. Amide and ester bond formation are also possibilities, but given the drug amphiphile requires a charged head-group (*eg*, lysine, glutamic or aspartic acids) there is a greater potential for unwanted side-reactions.

Last, the conditions required for purification of the final conjugate must not only be compatible with both the drug and the chosen linker group, but must also disfavor self-assembly of the conjugate since large aggregates will have poorer retention characteristics on reverse-phased silica when compared with the monomer.

To create a self-assembling drug amphiphile, we conjugated the DNA topoisomerase I inhibitor, camptothecin (Pommier, 2006 #4) to a β-sheet forming peptide derived from the Tau protein[77] –"C"GVQIVYKK ("C" indicates a cysteine-containing segment) (Scheme 1). The reducible disulfylbutyrate[8] moiety was chosen to link the two segments of the drug

amphiphile, employing the activated disulfide CPT-buSS-Pyr to direct disulfide bond formation with a cysteine-thiol of the peptide to form the conjugate (Scheme 2A). This linker can undergo reduction in the intracellular environment, breaking down to release the free drug. The two lysine residues at the *C*-terminal of the peptide serve as a hydrophilic head group to promote solubility and enable purification under acidic conditions, where assembly would be disrupted due to electrostatic repulsions[78]. The loading of the drug amphiphile can be precisely controlled by simply modifying the peptide design to incorporate multiple attachment sites. In our design, we used the two amine functionalities of lysine to introduce branching points at the *N*-terminal that were then functionalized with cysteine, allowing access to drug amphiphiles with 1, 2 or 4 drug molecules per conjugate (23%, 31% and 38% loadings, respectively, Scheme 2B).

From a practical standpoint, the branched peptides can be synthesized through conventional Fmoc solid-phase peptide synthesis procedures (Scheme 1). The only caveat to this, however, is that as the extent of branching increases (from one to four Cys attachment points), so too does the relative difficulty of achieving complete coupling. This can be attributed to the bulky Fmoc-Cys(tBu)-OH units being coupled to the branching lysines, with each subsequent addition increasing the steric bulk around the resin-bound peptide and hindering the approach of the next activated Cys residue to be added. Complete coupling was achieved through longer reaction times and repeated coupling with fresh reagents. Similar issues also arose when conjugating the CPT prodrug, as each addition will add a bulky CPT unit that can hinder further reaction for the di- and quad-substituted conjugates. Again, longer reaction time and a greater reagent excess were found to promote more complete conjugation.

**Effect of peptide segment on stability**

One property of the Tau conjugates described above that became apparent was how the solubility of the resultant conjugate is reduced with the increasing number of CPT molecules attached. mCPT-buSS-Tau was found to be very soluble, with solutions above 2 mol/L remaining clear, albeit with an increase in viscosity that led to gel formation. dCPT-buSS-Tau remained soluble up to 1 mol/L, becoming cloudy thereafter. qCPT-buSS-Tau on the other hand was sparingly soluble, giving a turbid solution even at 100 μmol/L. This observation may explain why only relatively short nanotubes were observed by TEM, as the availability of soluble monomers may reduce the likelihood of long nanotubes being formed, leading to formation of kinetically trapped short nanotubes.

One method to improve solubility is to incorporate a more hydrophilic peptide sequence. The Tau peptide is dominated by hydrophobic residues (Val and Ile) and as such may contribute to the poor solubility characteristics. We have synthesized analogues of dCPT-buSS-Tau and qCPT-buSS-Tau using a more hydrophilic β-sheet forming peptide derived from the Sup35 yeast prion, NNQQNY (Figure 4A)[79, 80], allowing a direct comparison of their properties. In the case of dCPT-buSS-Sup35[79], we saw little difference in the morphology formed with that of dCPT-buSS-Tau, giving nanofilamentous structures with widths of 8.9±1.3 nm—slightly wider than those of the Tau analogue. However, a clear difference was seen in the contour length, with the Sup35 conjugate forming fibrous nanostructures that were typically longer than 1 μm

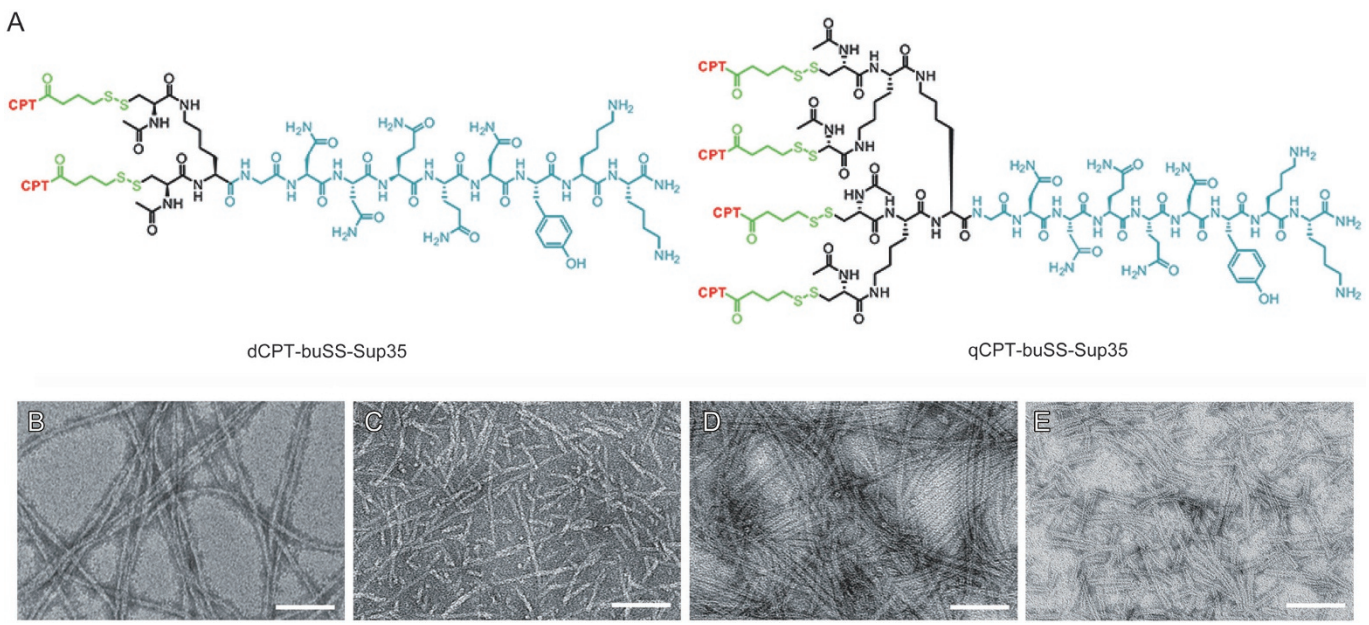


**Figure 4.** Comparison of CPT conjugates with Tau and Sup35 peptide segments. (A) Chemical structures of dCPT-buSS-Sup35 and qCPT-buSS-Sup35. Representative TEM images of dCPT-buSS-Sup35 (B), dCPT-buSS-Tau (C), qCPT-buSS-Sup35 (D) and qCPT-buSS-Tau (E). All samples are 100 μmol/L in $H_2O$, except for dCPT-buSS-Tau which is 200 μmol/L. Scale bars are 100 nm.

(Figure 4B), while the Tau conjugate formed predominantly shorter filaments (Figure 4C). Cryo-TEM imaging confirmed that these observations were not an artifact of the drying process involved in sample preparation (Supplementary Figure S9). A further effect of the more hydrophilic peptide was found in the apparent critical micellization concentrations (CMC), with that of dCPT-buSS-Sup35 being around 20–30 μmol/L in comparison to submicromolar for dCPT-buSS-Tau. This is borne out by the circular dichroism (CD) spectra of the two drug amphiphiles (Supplementary Figure S10), in which it can be clearly seen that the β-sheet signal of the Sup35 analogue is no longer apparent at 5 μmol/L, whereas that of the Tau conjugate is still present below 1 μmol/L. It is evident that the greater hydrophilicity of the Sup35 sequence lends a greater solubility to the resulting conjugate at the cost of a reduction in its propensity for self-assembly. Importantly, this effect on monomer solubility may provide a pathway for exerting some degree of control over the contour length of the one-dimensional nanostructures. This ability would be useful in tailoring the drug amphiphiles toward a particular application. Longer fibers are able to more effectively entangle than shorter fibers and would be ideal candidates for the formation of hydrogels, which can be utilized for local and sustained delivery of therapeutics[81–83]. On the other hand, shorter nanostructures would be more suitable for systemic delivery as they may fare better during circulation, being less likely to get trapped by the body's filtration mechanisms or in smaller capillary blood vessels.

Incorporation of the Sup35 peptide into the quad-CPT conjugate results in a marked improvement in the solubility[80], as clear solutions of the qCPT-buSS-Sup35 conjugate can be prepared that are above 1 mol/L in concentration. These solutions also exhibit greater viscosity, indicating the presence of longer nanostructures that can entangle. TEM imaging confirms the formation of nanotubes of widths 9.9±1.1 nm (Figure 4D), similar to those of qCPT-buSS-Tau (9.5±1.0 nm, Figure 4E), though a larger proportion were greater than 1 μm in length. The increased solubility the Sup35 peptide allows the nanotubes to further elongate during self-assembly. The hydrophobicity of the four CPT molecules clearly still plays an important role in the self-assembly, but the incorporation of the Sup35 peptide bestows a greater hydrophobic-hydrophilic balance to the conjugate that increases its solubility without compromising its stability.

Two concerns associated with β-sheet-based peptide assemblies are their potential toxicity and degradability for body clearance. In the case reported here, the two β-sheet segments we chose, Tau and Sup35, are derived from natural proteins known to form amyloid plaques. After conjugation with therapeutic agents and modification with charged amino acids, it is likely that their potential to induce formation of amyloid plaques is altered. In our *in vitro* studies with cells, although all the synthesized drug amphiphiles demonstrated effective toxicities against a number of cancer cell lines, no adverse effects were observed for filaments formed by self-assembly of the peptides conjugated with a linear hydrocarbon, suggesting the potential biocompatibility of the chosen peptide segments. However, for using these materials in an *in vivo* setting, more comprehensive studies are necessary to evaluate their unwanted toxicities in interfacing with other biomolecules. Further design of self-assembling drug amphiphiles should avoid using amyloid disease-related sequences as the auxiliary segment. Given the supramolecular nature of these filamentous assemblies, the concern related to their biodegradability is less an issue here, as we have demonstrated that these nanostructures can effectively release the incorporated therapeutic agents.

## Conclusion

In summary, we have detailed the guiding principles for the synthesis of anticancer drug amphiphiles, utilizing an established bioconjugation technique to create peptide-based prodrugs that can self-assemble into nanofibrous structures. The sequence of the conjugated peptide segment can not only be used to direct the self-assembly, but can also be utilized to control the solubility characteristics and influence the physicochemical properties of the resulting nanostructures. Given the range of hydrophobic anticancer drugs in current clinical use and the versatility present in peptide design, the approach we are developing has enormous potential as the basis for a future drug delivery platform.

## Acknowledgements

The work is supported by the National Science Foundation (DMR 1255281), USA. We thank National Institutes of Health (NIH) for funding Andrew G CHEETHAM (T-32CA130840). We acknowledge the use of the Johns Hopkins Department of Chemistry NMR and Mass Spectrometry Shared Facilities and the Integrated Imaging Center for access to the relevant instrumentation. Financial support for MALDI-Tof analysis was provided by NSF Grant CHE-0840463. We thank Dr Phil MORTIMER for assistance with LC-MS and Prof Kalina HRISTOVA for use of the CD spectropolarimeter.

## Author contribution

Andrew G CHEETHAM and Honggang CUI were responsible for the research design and data analysis; Andrew G CHEETHAM performed all syntheses, purifications, and molecular and spectroscopic characterizations; Yi-an LIN carried out TEM and Cryo-TEM imaging; Andrew G CHEETHAM, Ran LIN, and Honggang CUI wrote the paper.

## Supplementary Information

$^{1}$H and $^{13}$C NMR, HPLC chromatograms and mass spectrometric characterization of the purified materials can be found in the Supplementary Information on the website of Acta Pharmacologica Sinica.

## References

1 Lien S, Lowman HB. Therapeutic peptides. Trends Biotechnol 2003; 21: 556–62.

2 Albericio F, Kruger HG. Therapeutic peptides. Future Med Chem

2012; 4: 1527–31.
3 Ahrens VM, Bellmann-Sickert K, Beck-Sickinger AG. Peptides and peptide conjugates: therapeutics on the upward path. Future Med Chem 2012; 4: 1567–86.
4 Arap W, Pasqualini R, Ruoslahti E. Cancer treatment by targeted drug delivery to tumor vasculature in a mouse model. Science 1998; 279: 377–80.
5 Burkhart DJ, Kalet BT, Coleman MP, Post GC, Koch TH. Doxorubicin-formaldehyde conjugates targeting $\alpha_v\beta_3$ integrin. Mol Cancer Ther 2004; 3: 1593–604.
6 Wang S, Placzek WJ, Stebbins JL, Mitra S, Noberini R, Koolpe M, *et al.* Novel targeted system to deliver chemotherapeutic drugs to EphA2-expressing cancer cells. J Med Chem 2012; 55: 2427–36.
7 Brooks H, Lebleu B, Vives E. Tat peptide-mediated cellular delivery: back to basics. Adv Drug Deliv Rev 2005; 57: 559–77.
8 Dubikovskaya EA, Thorne SH, Pillow TH, Contag CH, Wender PA. Overcoming multidrug resistance of small-molecule therapeutics through conjugation with releasable octaarginine transporters. Proc Natl Acad Sci U S A 2008; 105: 12128–33.
9 Soukasene S, Toft DJ, Moyer TJ, Lu HM, Lee HK, Standley SM, *et al.* Antitumor activity of peptide amphiphile nanofiber-encapsulated camptothecin. ACS Nano 2011; 5: 9113–21.
10 Zhang PC, Cheetham AG, Lock LL, Cui HG. Cellular uptake and cytotoxicity of drug-peptide conjugates regulated by conjugation site. Bioconjugate Chem 2013; 24: 604–13.
11 Wang Y, Cheetham AG, Angacian G, Su H, Xie L, Cui H. Peptide-drug conjugates as effective prodrug strategies for targeted delivery. Adv Drug Deliv Rev 2016; pii: S0169-409X(16)30208-3.
12 Lin R, Zhang PC, Cheetham AG, Walston J, Abadir P, Cui HG. Dual peptide conjugation strategy for improved cellular uptake and mitochondria targeting. Bioconjugate Chem 2015; 26: 71–7.
13 Zompra AA, Galanis AS, Werbitzky O, Albericio F. Manufacturing peptides as active pharmaceutical ingredients. Future Med Chem 2009; 1: 361–77.
14 Su H, Koo JM, Cui HG. One-component nanomedicine. J Control Release 2015; 219: 383–95.
15 Hartgerink JD, Beniash E, Stupp SI. Self-assembly and mineralization of peptide-amphiphile nanofibers. Science 2001; 294: 1684–8.
16 Rajangam K, Behanna HA, Hui MJ, Han XQ, Hulvat JF, Lomasney JW, *et al.* Heparin binding nanostructures to promote growth of blood vessels. Nano Lett 2006; 6: 2086–90.
17 Standley SM, Toft DJ, Cheng H, Soukasene S, Chen J, Raja SM, *et al.* Induction of cancer cell death by self-assembling nanostructures incorporating a cytotoxic peptide. Cancer Res 2010; 70: 3020–6.
18 Pakalns T, Haverstick KL, Fields GB, McCarthy JB, Mooradian DL, Tirrell M. Cellular recognition of synthetic peptide amphiphiles in self-assembled monolayer films. Biomaterials 1999; 20: 2265–79.
19 Trent A, Marullo R, Lin B, Black M, Tirrell M. Structural properties of soluble peptide amphiphile micelles. Soft Matter 2011; 7: 9572–82.
20 Jun HW, Yuwono V, Paramonov SE, Hartgerink JD. Enzyme-mediated degradation of peptide-amphiphile nanofiber networks. Adv Mater 2005; 17: 2612–7.
21 Gauba V, Hartgerink JD. Self-assembled heterotrimeric collagen triple helices directed through electrostatic interactions. J Am Chem Soc 2007; 129: 2683–90.
22 Toledano S, Williams RJ, Jayawarna V, Ulijn RV. Enzyme-triggered self-assembly of peptide hydrogels via reversed hydrolysis. J Am Chem Soc 2006; 128: 1070–1.
23 Smith AM, Williams RJ, Tang C, Coppo P, Collins RF, Turner ML, *et al.* Fmoc-Diphenylalanine self assembles to a hydrogel via a novel architecture based on pi-pi interlocked beta-sheets. Adv Mater 2008; 20: 37–41.
24 Ceylan H, Tekinay AB, Guler MO. Selective adhesion and growth of vascular endothelial cells on bioactive peptide nanofiber functionalized stainless steel surface. Biomaterials 2011; 32: 8797–805.
25 Cinar G, Ceylan H, Urel M, Erkal TS, Tekin ED, Tekinay AB, *et al.* Amyloid inspired self-assembled peptide nanofibers. Biomacromolecules 2012; 13: 3377–87.
26 Schneider JP, Pochan DJ, Ozbas B, Rajagopal K, Pakstis L, Kretsinger J. Responsive hydrogels from the intramolecular folding and self-assembly of a designed peptide. J Am Chem Soc 2002; 124: 15030–7.
27 Li JY, Kuang Y, Gao Y, Du XW, Shi JF, Xu B. D-amino acids boost the selectivity and confer supramolecular hydrogels of a nonsteroidal anti-inflammatory drug (NSAID). J Am Chem Soc 2013; 135: 542–5.
28 Cheetham AG, Keith D, Zhang PC, Lin R, Su H, Cui HG. Targeting tumors with small molecule peptides. Curr Cancer Drug Targets 2016; 16: 489–508.
29 Su H, Zhang PC, Cheetham AG, Koo JM, Lin R, Masood A, *et al.* Supramolecular crafting of self-assembling camptothecin prodrugs with enhanced efficacy against primary cancer cells. Theranostics 2016; 6: 1065–74.
30 Lock LL, Tang Z, Keith D, Reyes C, Cui HG. Enzyme-specific doxorubicin drug beacon as drug-resistant theranostic molecular probes. ACS Macro Lett 2015; 4: 552–5.
31 Sievers EL, Linenberger M. Mylotarg: Antibody-targeted chemotherapy comes of age. Curr Opin Oncol 2001; 13: 522–7.
32 Younes A, Yasothan U, Kirkpatrick P. Brentuximab vedotin. Nat Rev Drug Discov 2012; 11: 19–20.
33 Traynor K. Ado-trastuzumab emtansine approved for advanced breast cancer. Am J Health Sys Pharm 2013; 70: 562.
34 Vlieghe P, Lisowski V, Martinez J, Khrestchatisky M. Synthetic therapeutic peptides: science and market. Drug Discov Today 2010; 15: 40–56.
35 Tang L, Persky AM, Hochhaus G, Meibohm B. Pharmacokinetic aspects of biotechnology products. J Pharm Sci 2004; 93: 2184–204.
36 Evans WE, Relling MV. Clinical pharmacokinetics-pharmacodynamics of anticancer drugs. Clin Pharmacokinet 1989; 16: 327–36.
37 Undevia SD, Gomez-Abuin G, Ratain MJ. Pharmacokinetic variability of anticancer agents. Nat Rev Cancer 2005; 5: 447–58.
38 Duncan R. Polymer conjugates as anticancer nanomedicines. Nat Rev Cancer 2006; 6: 688–701.
39 Tong R, Cheng J. Anticancer polymeric nanomedicines. Polym Rev 2007; 47: 345–81.
40 Cheng JJ, Khin KT, Jensen GS, Liu AJ, Davis ME. Synthesis of linear, beta-cyclodextrin-based polymers and their camptothecin conjugates. Bioconjugate Chem 2003; 14: 1007–17.
41 Zou J, Jafr G, Themistou E, Yap Y, Wintrob ZAP, Alexandridis P, *et al.* pH-Sensitive brush polymer-drug conjugates by ring-opening metathesis copolymerization. Chem Commun 2011; 47: 4493–5.
42 Yu Y, Chen CK, Law WC, Mok J, Zou J, Prasad PN, *et al.* Well-defined degradable brush polymer-drug conjugates for sustained delivery of paclitaxel. Mol Pharm 2013; 10: 867–74.
43 Gao Y, Kuang Y, Guo ZF, Guo ZH, Krauss IJ, Xu B. Enzyme-instructed molecular self-assembly confers nanofibers and a supramolecular hydrogel of taxol derivative. J Am Chem Soc 2009; 131: 13576–7.
44 Shen Y, Jin E, Zhang B, Murphy CJ, Sui M, Zhao J, *et al.* Prodrugs forming high drug loading multifunctional nanocapsules for intracellular cancer drug delivery. J Am Chem Soc 2010; 132: 4259–65.
45 Cheetham AG, Zhang P, Lin YA, Lock LL, Cui H. Supramolecular nanostructures formed by anticancer drug assembly. J Am Chem Soc

2013; 135: 2907–10.
46 Lin R, Cheetham AG, Zhang P, Lin YA, Cui H. Supramolecular filaments containing a fixed 41% paclitaxel loading. Chem Commun (Camb) 2013; 49: 4968–70.
47 Li XY, Yang CB, Zhang ZL, Wu ZD, Deng Y, Liang GL, *et al.* Folic acid as a versatile motif to construct molecular hydrogelators through conjugations with hydrophobic therapeutic agents. J Mater Chem 2012; 22: 21838–40.
48 Wang HM, Wei J, Yang CB, Zhao HY, Li DX, Yin ZN, *et al.* The inhibition of tumor growth and metastasis by self-assembled nanofibers of taxol. Biomaterials 2012; 33: 5848–53.
49 McDaniel JR, Bhattacharyya J, Vargo KB, Hassouneh W, Hammer DA, Chilkoti A. Self-assembly of thermally responsive nanoparticles of a genetically encoded peptide polymer by drug conjugation. Angew Chem Int Ed 2013; 52: 1683–7.
50 Lock LL, Reyes CD, Zhang PC, Cui HG. Tuning cellular uptake of molecular probes by rational design of their assembly into supramolecular nanoprobes. J Am Chem Soc 2016; 138: 3533–40.
51 Lin R, Cui HG. Supramolecular nanostructures as drug carriers. Curr Opin Chem Eng 2015; 7: 75–83.
52 Hu XY, Liu X, Zhang WY, Qin S, Yao CH, Li Y, *et al.* Controllable construction of biocompatible supramolecular micelles and vesicles by water-soluble phosphate pillar 5,6 arenes for selective anti-cancer drug delivery. Chem Mater 2016; 28: 3778–88.
53 Tan XY, Lu XG, Jia F, Liu XF, Sun YH, Logan JK, *et al.* Blurring the role of oligonucleotides: spherical nucleic acids as a drug delivery vehicle. J Am Chem Soc 2016; 138: 10834–7.
54 Sun Y, Kaplan JA, Shieh A, Sun HL, Croce CM, Grinstaff MW, *et al.* Self-assembly of a 5-fluorouracil-dipeptide hydrogel. Chem Commun 2016; 52: 5254–7.
55 Sun Y, Shieh A, Kim SH, King S, Kim A, Sun HL, *et al.* The self-assembly of a camptothecin-lysine nanotube. Bioorg Med Chem Lett 2016; 26: 2834–8.
56 Zhou Z, Munyaradzi O, Xia X, Green D, Bong D. High-capacity drug carriers from common polymer amphiphiles. Biomacromolecules 2016; 17: 3060–6.
57 Pommier Y. Topoisomerase I inhibitors: camptothecins and beyond. Nat Rev Cancer 2006; 6: 789–802.
58 Cheetham AG, Ou YC, Zhang PC, Cui HG. Linker-determined drug release mechanism of free camptothecin from self-assembling drug amphiphiles. Chem Commun 2014; 50: 6039–42.
59 Kang M, Zhang PC, Cui HG, Loverde SM. pi-pi Stacking mediated chirality in functional supramolecular filaments. Macromolecules 2016; 49: 994–1001.
60 Cui HG, Webber MJ, Stupp SI. Self-assembly of peptide amphiphiles: from molecules to nanostructures to biomaterials. Biopolymers 2010; 94: 1–18.
61 Hauser CAE, Zhang S. Designer self-assembling peptide nanofiber biological materials. Chem Soc Rev 2010; 39: 2780–90.
62 Kimura S, Kim DH, Sugiyama J, Imanishi Y. Vesicular self-assembly of a helical peptide in water. Langmuir 1999; 15: 4461–3.
63 Santoso S, Hwang W, Hartman H, Zhang SG. Self-assembly of surfactant-like peptides with variable glycine tails to form nanotubes and nanovesicles. Nano Lett 2002; 2: 687–91.
64 Jaracz S, Chen J, Kuznetsova LV, Ojima L. Recent advances in tumor-targeting anticancer drug conjugates. Bioorg Med Chem 2005; 13: 5043–54.
65 Byrne JD, Betancourt T, Brannon-Peppas L. Active targeting schemes for nanoparticle systems in cancer therapeutics. Adv Drug Deliv Rev 2008; 60: 1615–26.
66 Peng MY, Qin SY, Jia HZ, Zheng DW, Rong L, Zhang XZ. Self-delivery of a peptide-based prodrug for tumor-targeting therapy. Nano Res 2016; 9: 663–73.
67 Knop K, Hoogenboom R, Fischer D, Schubert US. Poly(ethylene glycol) in drug delivery: pros and cons as well as potential alternatives. Angew Chem Int Ed 2010; 49: 6288–308.
68 Sosnik A. Drug self-assembly: A phenomenon at the nanometer scale with major impact in the structure-biological properties relationship and the treatment of disease. Prog Mater Sci 2016; 82: 39–82.
69 MacKay JA, Chen M, McDaniel JR, Liu W, Simnick AJ, Chilkoti A. Self-assembling chimeric polypeptide-doxorubicin conjugate nanoparticles that abolish tumours after a single injection. Nat Mater 2009; 8: 993–9.
70 Dubowchik GM, Firestone RA. Cathepsin B-sensitive dipeptide prodrugs. 1. A model study of structural requirements for efficient release of doxorubicin. Bioorg Med Chem Lett 1998; 8: 3341–6.
71 Dubowchik GM, Mosure K, Knipe JO, Firestone RA. Cathepsin B-sensitive dipeptide prodrugs. 2. Models of anticancer drugs paclitaxel (Ttaxol (R)), mitomycin C and doxorubicin. Bioorg Med Chem Lett 1998; 8: 3347–52.
72 Cheng R, Feng F, Meng F, Deng C, Feijen J, Zhong Z. Glutathione-responsive nano-vehicles as a promising platform for targeted intracellular drug and gene delivery. J Control Release 2011; 152: 2–12.
73 Zhong T, Huang R, Tan LJ. Amphiphilic drug-drug assembly via dual-responsive linkages for small-molecule anticancer drug delivery. RSC Advances 2016; 6: 66420–30.
74 Andreu D, Albericio F, Sole NA, Munson MC, Ferrer M, Barany G. Formation of disulfide bonds in synthetic peptides and proteins. Meth Mol Biol 1994; 35: 91–169.
75 Hoyle CE, Bowman CN. Thiol-ene click chemistry. Angew Chem Int Ed 2010; 49: 1540–73.
76 Lutz JF, Zarafshani Z. Efficient construction of therapeutics, bioconjugates, biomaterials and bioactive surfaces using azide-alkyne "click" chemistry. Adv Drug Deliv Rev 2008; 60: 958–70.
77 Goux WJ, Kopplin L, Nguyen AD, Leak K, Rutkofsky M, Shanmuganandam VD, *et al.* The formation of straight and twisted filaments from short tau peptides. J Biol Chem 2004; 279: 26868–75.
78 Hu Y, Lin R, Patel K, Cheetham AG, Kan CY, Cui HG. Spatiotemporal control of the creation and immolation of peptide assemblies. Coord Chem Rev 2016; 320: 2–17.
79 Cheetham AG, Zhang P, Lin YA, Lin R, Cui H. Synthesis and self-assembly of a mikto-arm star dual drug amphiphile containing both paclitaxel and camptothecin. J Mater Chem B 2014; 2: 7316–26.
80 Lin YA, Cheetham AG, Zhang PC, Ou YC, Li YG, Liu GS, *et al.* Multi-walled nanotubes formed by catanionic mixtures of drug amphiphiles. ACS Nano 2014; 8: 12690–700.
81 Du XW, Zhou J, Shi JF, Xu B. Supramolecular hydrogelators and hydrogels: from soft matter to molecular biomaterials. Chem Rev 2015; 115: 13165–307.
82 Luo Y, Li M, Zhao YW, Liu H, Gong TX, Hong Y, *et al.* Molecular nanofibers of paclitaxel form supramolecular hydrogel for preventing tumor growth *in vivo*. RSC Advances 2016; 6: 80847–50.
83 Peltier R, Chen GC, Lei HP, Zhang M, Gao LQ, Lee SS, *et al.* The rational design of a peptide-based hydrogel responsive to $H_2S$. Chem Commun 2015; 51: 17273–6.